Molecular Plant • Volume 2 • Number 1 • Pages 138–151 • January 2009 RESEARCH ARTICLE

HOS3, an ELO-Like Gene, Inhibits Effects of ABA and Implicates a S-1-P/Ceramide Control System for Abiotic Stress Responses in *Arabidopsis thaliana*

Tanya M. Quist[a], Irina Sokolchik[a], Huazhong Shi[b], Robert J. Joly[a], Ray A. Bressan[a], Albino Maggio[c], Meena Narsimhan[a] and **Xia Li[d,1]**

a Center for Plant Environmental Stress Physiology, Purdue University, West Lafayette, IN 47907-2010, USA
b Department of Chemistry and Biochemistry, Texas Tech University, Lubbock, TX 79409-1061, USA
c Department of Agricultural Engineering and Agronomy, University of Naples Federico II, Via Università 100, Portici (NA), Italy 80055
d The Key Laboratory of Plant Cell and Chromosome Engineering, Institute of Genetics and Developmental Biology, Chinese Academy of Sciences, Shijiazhuang, Hebei, 050021 China

ABSTRACT A hyper-osmotically sensitive mutant of *Arabidopsis thaliana*, designated *hos3-1* (*high expression of osmotically responsive genes*), was identified based on its hyper-luminescence of *RD29A:LUC* promoter fusion plants upon treatment with NaCl and ABA. These responses implicate the disrupted gene as a direct or indirect negative regulator of the *RD29A* stress-responsive pathway. By sequencing the flanking regions of the T-DNA borders, it was determined that the disrupted gene is at locus At4g36830, annotated as encoding a putative protein with high homology to *CIG30* (*ELO2*/*FEN1*). CIG30 has been implicated in synthesis of very long chain fatty acids (VLCFA), which are essential precursors for sphingolipids and ceramides. Altered stress responses characteristic of ABA-hypersensitivity, including reduced root growth inhibition and reduced germination with ABA treatment and reduced water loss from leaves, were exhibited by allelic *hos3-1* and *hos3-2* mutants. The *hos3-2* mutant is partially suppressed in its transcript abundance and is inherited as a recessive trait. Further, the *HOS3* ORF under the control of the 35SCaMV promoter restored wild-type NaCl- and ABA-root growth sensitivity as well as *RD29A*:*LUC* luminescence in mutant plants. We also show here that the *HOS3* wild-type gene functionally complements the sensitivity of *elo2* and *elo3* yeast mutants to monensin. Furthermore, both *hos3-1* and *hos3-2* alleles shared increased sensitivity to the herbicide Metolachlor, which inhibits acyl chain elongation in synthesis of VLCFA, and *HOS3* functionally complemented both *elo2* and *elo3* and restored levels of VLCFA. Together, these data establish that HOS3 inhibits ABA-mediated stress responses and implicate the VLCFA pathway and products as control points for several aspects of abiotic stress signaling and responses. The results also provide support for a role of ceramide in the control of stomatal behavior.

Key words: Abiotic stress; *Arabidopsis*; ABA signal pathway; stomata; very long chain fatty acid pathway.

INTRODUCTION

Lipids serve as hydrophobic barriers that confer structural integrity to cells and organelles in addition to their role as a major form of chemical energy. More than 90% of plant and animal lipids comprise fatty acid species with a maximum chain length of 18 carbons (Holthuis et al., 2001; Merrill, 2002; Leonard et al., 2004). However, a class of lipids known as very long chain fatty acids (VLCFA) comprise fatty acid chain lengths greater than 20 carbons. The VLCFA are ubiquitous (Tvrdik et al., 2000; Pyne and Pyne, 2000) and are most often esterified in various lipids or they are amide-linked to the long-chain sphingoid base, sphinganine (Sph) (Tvrdik et al., 2000), to form the plasma membrane localized sphingolipids. Sphingolipids are typically found in eukaryotic cells, where they comprise

[1] To whom correspondence should be addressed. E-mail xli@genetics.ac.cn, tel. 86-0311-85871744.

doi: 10.1093/mp/ssn085
Received 9 September 2008; accepted 3 November 2008

a small but vital fraction (10–20%) of the membrane lipids (Holthuis et al., 2001). In yeast and mammals, sphingolipids facilitate cell recognition and adhesion via complex sugar groups, docking and fusion of secretory vesicles and also contribute to membrane stability as principal components of the membrane microdomains (lipid rafts) (Brown and London, 2000; Worrall et al., 2003). As major components of lipid rafts, sphingolipids may mediate protein sorting events to bring about differential membrane composition, which has long been believed to be based solely on protein–protein interactions. In support of this possibility, sphingolipid synthesis occurs in the Golgi apparatus, which is also the central sorting station along the secretory pathway, and sphingolipids have been attributed as central to the sorting function of this organelle (Holthuis et al., 2001). This evidence suggests an interplay between both protein- and lipid-mediated sorting (Holthuis et al., 2001).

Sphingolipids also serve essential roles as signaling molecules that control many cellular processes, including growth, cell proliferation, apoptosis, pathogenesis and stress responses (Van Brocklyn et al., 1998; Kolesnick and Kronke, 1998; Spiegel and Milstien, 2000, 2002; Merrill, 2002; Sperling and Heinz, 2003; Worrall et al., 2003). VLCFA, specifically, confer essential function in sphingolipid signaling, since glycerophospholipids containing VLCFA can mimic sphingolipid structures and complement sphingolipid-deficient yeast (Lester et al., 1993; Lester and Dickson, 1993). Of particular importance in signaling are the sphingolipid metabolites ceramide, sphingosine and sphingosine-1-phosphate (S-1-P) (Ng et al., 2001). In mammals, S-1-P functions as both an intracellular messenger and an extracellular ligand for G-protein coupled receptors that regulate diverse biological processes ranging from cell proliferation to apoptosis (Hakomori and Igarashi, 1995; Kolesnick and Kronke, 1998; Spiegel and Milstien, 2000, 2002; Pyne and Pyne, 2000; Merrill, 2002).

Studies in plants have yielded results indicating regulatory functions for VLCFA, sphingolipids and ceramides as in mammals and yeast (Dunn et al., 2004; Leonard et al., 2004). There is genetic and biochemical evidence associating the in-planta level of VLCFAs or VLCFA derivatives with the magnitude of hypersensitive cell death response to pathogen attack (Raffaele et al., 2008). The transcription factor MYB30 was found to control the acyl–coA elongase complex that participates in the synthesis of very-long-chain fatty acids (VLCFAs) and also the hypersensitive response to pathogen attack. Because the exaggerated HR phenotype of *MYB30*-overexpressing lines was negated by limiting the supply of precursors for VLCFA biosynthesis by a loss-of-function mutation in the acyl–ACP thioesterase FATB, it has been proposed that VLCFAs or VLCFA derivatives may function as cell death messengers in the hypersensitive response to pathogen attack. VLCFA biosynthesis also significantly affects elongation of cotton fiber (*Gossypium hirsutum*), cell elongation in *Arabidopsis* and normal embryo development in corn (Zheng et al., 2005; Qin et al., 2007; Dietrich et al., 2005). Phenotypes of *Arabidopsis* mutants bearing null mutations in genes encoding isoenzymes catalyzing the initial committed step in VLCFA biosynthesis show that these proteins have a role in controlling organ development and stomatal density (Millar et al., 1999; Gray et al., 2000; Pruitt et al., 2000) and imply that VLCFAs and/or their derivatives, such as sphingolipid and ceramides, have important roles in the mediation of signaling in plants.

Indeed, studies in *Arabidopsis thaliana* have shown that sphingosine-1-phosphate (S-1-P) and phytosphingosine-1-phosphate function as intracellular messengers in response to the plant stress hormone abscisic acid (ABA). ABA stimulates sphingosine kinase (SPHK), the enzyme responsible for S-1-P production (Coursol et al., 2003, 2005; Worrall et al., 2008). Incubation of epidermal strips of *Commelina communis* with S-1-P promoted reversible closure of stomata (Ng et al., 2001), and stimulation of S-1-P synthesis by ABA led to reduction in stomatal aperture in *Arabidopsis* (Coursol et al., 2005). Genetic evidence supports involvement of S-1-P upstream of heterotrimeric G-protein signaling in several ABA-mediated biological processes, such as stomatal responses and seed germination (Coursol et al., 2003, 2005; Worrall et al., 2008). The stomata of SPHK1 knock-down *Arabidopsis* plants were less sensitive to ABA, whereas the stomata of SPHK1-overexpression lines were more sensitive than those of the wild-type plants. Germination rate was reduced by SPHK1 knock-down and increased by SPHK1 overexpression (Worrall et al., 2008). Regulation of stomatal aperture and ion channel activities in guard cells by S-1-P was abrogated by null mutation of the alpha subunit of the sole heterotrimeric G-protein of *Arabidopsis* (Wang et al., 2001). Ceramides are sphinosine derivatives composed of sphingosine and a fatty acid. They are known to induce programmed cell death in animals. Ceramide also induces programmed cell death in *Arabidopsis* (Liang et al., 2003; Townley et al., 2005). This was demonstrated by adding ceramide directly to cultured cells or protoplasts. Evidence for the *in-vivo* involvement of ceramide in programmed cell death comes from the accelerated cell death phenotype of *acd5* mutants of *Arabidopsis* that lack ceramide kinase, an enzyme that converts phosphorylates and thereby inactivates ceramide (Liang et al., 2003).

In plants and yeast, fatty acid synthesis usually terminates with C16:0 or C18:0 products. VLCFA are derived from the sequential addition of 2-carbon units to the products of de-novo fatty acid biosynthesis through a cyclic series of reactions that involves a 3-ketoacyl-CoA synthase, a 3-ketoacyl-CoA reductase, a dehydrase, and an enoyl-CoA reductase (Blacklock and Jaworski, 2006; Tehlivets et al., 2007). The details of the genes and proteins involved in these processes are not fully understood in either yeast or plants. The condensation of fatty acyl-CoA with malonyl-CoA that is catalyzed by 3-ketoacyl-CoA synthase is the first and rate-limiting step in the biosynthesis of VLCFA. In yeast, the homologous proteins ELO1, ELO2, and ELO3 are required for this process, although evidence that they have enzymatic activity is missing. The ELO proteins differ in the chain length specificity of their fatty acyl CoA substrates, with ELO1 being specific for medium, long-chain and

monounsaturated fatty acyl-CoA, ELO2 elongating up to C_{22} and ELO3 up to C_{26}. Plant 3-ketoacyl-CoA synthases are referred to as FAE1-KCS (fatty acid elongase 1 3-ketoacyl-CoA synthase). There are 21 known and putative KCSs in *Arabidopsis*. Although plant KCSs have no known homologs in yeast, several *Arabidopsis* FAE1-KCSs are able to direct VLCFA synthesis in yeast and several rescue the lethality of Δ*elo2*Δ*elo3* mutation in yeast (Paul et al., 2006). Although *Arabidopsis* FAE1-KCSs and yeast ELO proteins have similar functions, they are structurally dissimilar. The FAE1-KCS proteins have a conserved active site cysteine, histidine, and asparagine that is missing in the ELO proteins. The ELOs on the other hand contain a highly conserved histidine box that is suggestive of a metal binding site that is missing in the FAE1-KCSs. The ELO proteins are predicted to have five to seven transmembrane domains spread over the proteins, whereas the FAE1-KCSs only have two membrane spanning regions at the N-terminus (Paul et al., 2006). We report here that an ELO3-like gene in *Arabidopsis thaliana*, designated *HOS3*, controls VLCFA composition and functions to inhibit ABA-mediated stress responses, including regulation of stomatal aperture, maintenance of primary root growth and inhibition of germination. *HOS3* complements the monensin sensitivity of yeast *elo2* and *elo3* mutants, and also controls VLCFA composition in yeast. These results provide new information on VLCFA biosynthesis in plants and demonstrate the involvement of ELO-like plant proteins in this process. They also support a role for VLCFA as signaling components acting upstream of S-1-P, ceramide and the heterotrimeric G-protein complex, in lipid-mediated regulation of abiotic stress signaling in plants.

RESULTS

RD29A:LUC Luminescence in *hos3-1* is Hyper-Induced by Osmotic Stress and ABA

Comparing *RD29A:LUC* transgene expression of the *hos3-1* T_3 generation seedlings with wild-type plants by CCD imaging revealed hyper-induction of the transgene in *hos3-1* by NaCl (300 mM) or ABA (100 μM). No significant change in expression was detected in response to low-temperature treatment (Figure 1A and 1B). Enhanced transcript abundance of the native *RD29A* gene in both *hos3-1* and *hos3-2* mutants, with and without NaCl treatment, was consistent with increases in LUC luminescence visualized (data not shown).

HOS3 Attenuates Root Growth under Osmotic Stress

The magnitude of difference in primary root growth of *hos3-1* compared with wild-type C24 (*RD29A:LUC*) increased with increasing concentrations of NaCl. Primary root growth in mutant

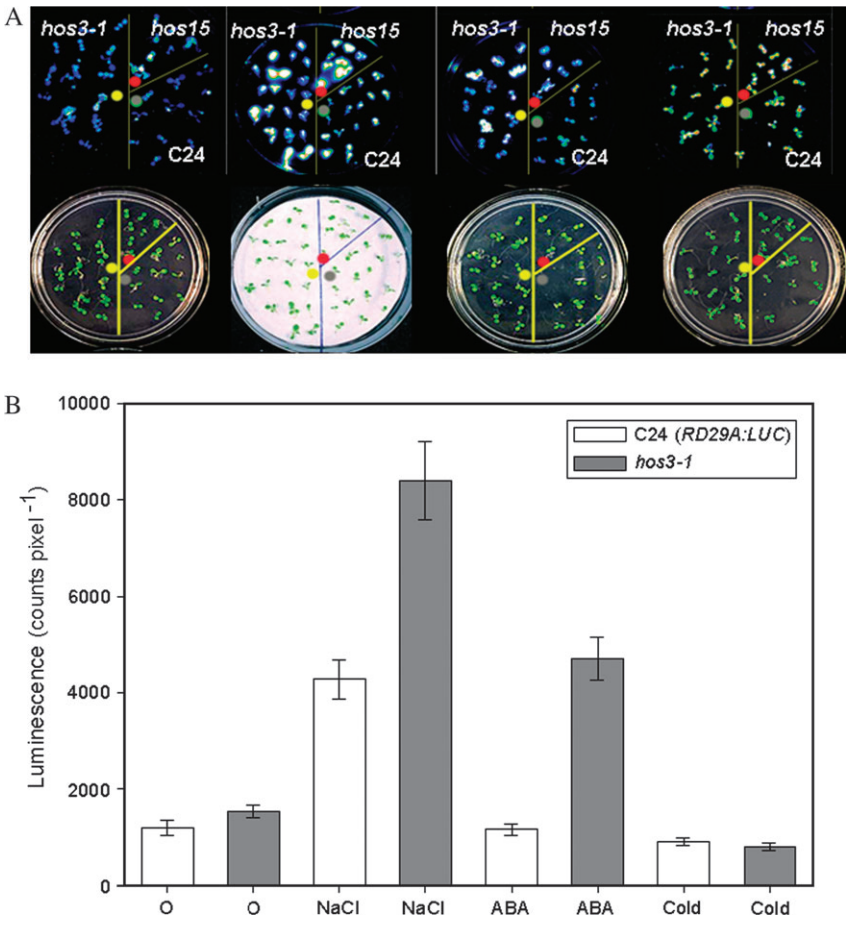

Figure 1. *RD29A:LUC* Luminescence Is Hyper-Induced by Osmotic Stress in *hos3-1*.

(A) Seedlings on plates (bottom frames) and respective luminescence images (top frames) were treated with 300 mM NaCl, 100 μM ABA or 24 h cold treatment at 0°C from left to right. *hos15* was used as a positive control.

(B) Sensitivity to stress of *hos3-1* was determined by comparing the luminescence of the mutant seedlings (grey bars) with that of the wild-type C24 (*RD29A:LUC*) (open bars) after treatment with 300 mM NaCl, 100 μM ABA or 24 h cold treatment at 0°C. Means and standard errors were determined by ANOVA with a confidence interval of $\alpha = 0.05$. Error bars represent ±1 SE.

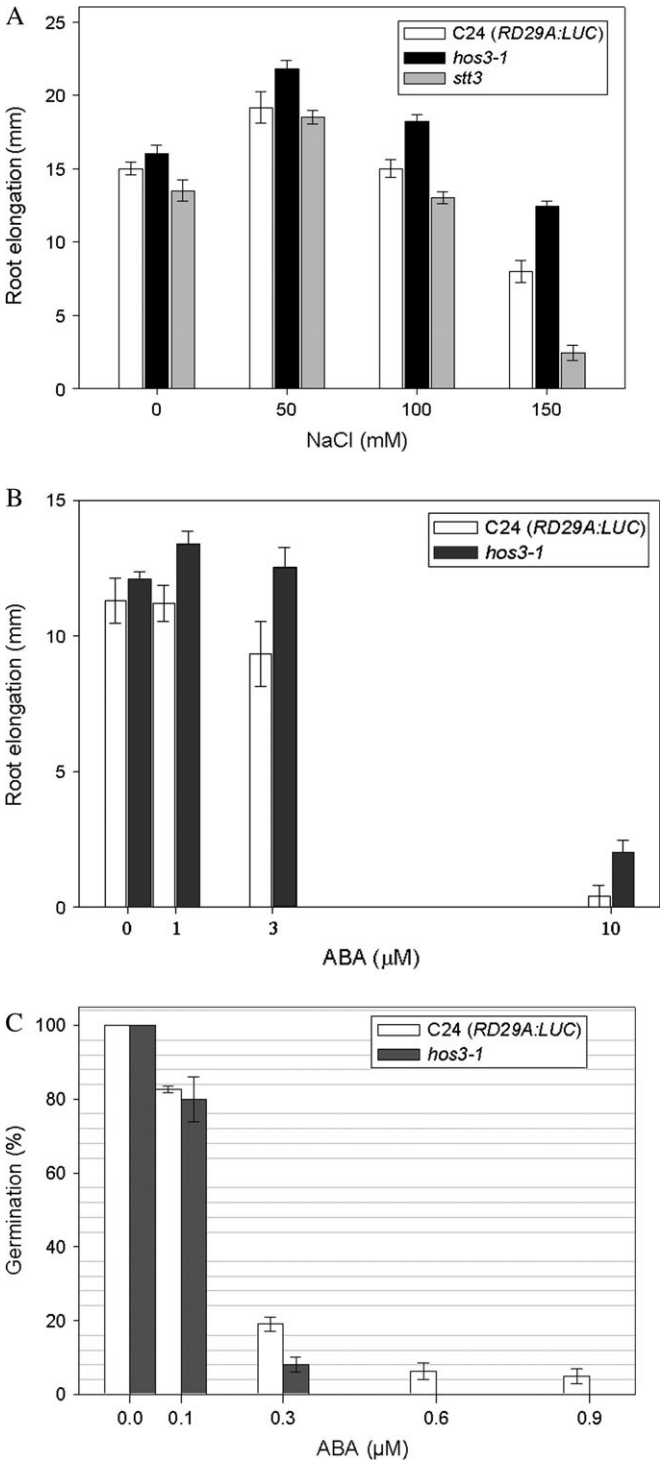

Figure 2. *hos3-1* Functionally Disrupts Salt Stress Responses.

(A) Root elongation of C24 (*RD29A:LUC*) (open bars) and *hos*3-*1* (black bars) on media containing NaCl (0, 50, 100, or 150 mM) were compared with the NaCl and osmotically sensitive *stt*3 (grey bars) mutant (Koiwa et al., 2003). Statistical analysis was performed using ANOVA function to compare root growth elongation with a confidence interval of $\alpha = 0.05$. Error bars represent $\pm$1 SE.

plants was 12.2, 17.8, and 35.5% greater than growth of wild-type with 50, 100, and 150 mM NaCl, respectively (Figure 2A). Osmotic sensitivity was similarly resistant as *hos3-1* primary root growth after 6 d on mannitol-containing media was 13% greater than wild-type, both equal and opposite to the osmotically sensitive *stt*3 mutant (Koiwa et al., 2003) (data not shown). Enhanced root growth upon osmotic stress is consistent with HOS3 functioning as a negative regulator of stress-induced root growth inhibition, or as an inhibitor of ABA, which maintains primary root growth under stress. Similarly, root growth in *hos3-1* upon treatment with 3 μM ABA was 20% greater compared with wild-type C24 (*RD29A:LUC*) (Figure 2B). This result suggests HOS3 exerts its negative effect on root growth in an ABA-dependent manner.

HOS3 Negatively Regulates ABA Inhibition of Germination

Consistent with HOS3 functioning as an ABA-inhibitor, ABA-inhibition of seed dormancy, measured as germination rate of *hos3-1* mutant seeds on 0.3 μM ABA, was half of that measured for wild-type (Figure 2C). Further, no mutant seeds were able to germinate at higher concentrations of ABA ($>$0.6 μM), though wild-type continued to germinate at a low rate.

HOS3 Regulates Stomatal Aperture

Water loss rates of intact *hos3-1* seedlings were consistently lower than wild-type when unstressed. During the light period, mean difference in water loss in the *hos3-1* mutant was approximately 13% lower than wild-type (Figure 3A). C24 (*RD29A:LUC*) wild-type and *hos3-1* leaves, left untreated or treated with ABA, were excised and examined for changes in rate of water loss over time. Excised shoots from untreated mutant plants maintained 12% higher water content compared to wild-type controls, indicating enhanced stomatal closure in *hos3-1* mutants (Figure 3B). When treated with ABA prior to excision, leaves of *hos3-1* plants lost 10% more water compared with wild-type (Figure 3C). However, comparison of the relative difference in ABA-response between mutant and wild-type among ABA-treated groups revealed that while wild-type C24(*RD29A:LUC*) lost approximately 21% less water, *hos3-1* mutant water loss was less affected by ABA treatment, with only a 4% reduction compared to untreated mutant response (Figure 3D). Considered together, these results indicate that HOS3 may negatively regulate ABA-mediated stomatal aperture.

Identification of the hos3-1 Locus

TAIL-PCR, to sequence the flanking region of the T-DNA insert in *hos3-1*, confirmed an insertion in At4g36830, annotated as

(B) Root elongation of C24 (*RD29A:LUC*) wild-type (open bars) was compared with *hos*3-*1* (dark grey bars) seedlings after 6 d growth on media containing ABA (0, 1, 3, or 10 μM).

(C) T_3 seeds of *hos3-1* (dark grey bars) and wild-type C24 (*RD29A:-LUC*) (open bars) were plated onto ½ $\times$ MS media (1.0% agar) containing ABA (0, 0.1, 0.3, 0.6, or 0.9 μM). The mean number of plants germinated after 9 d were plotted relative to the number of plants germinated on control medium and expressed as a percent.

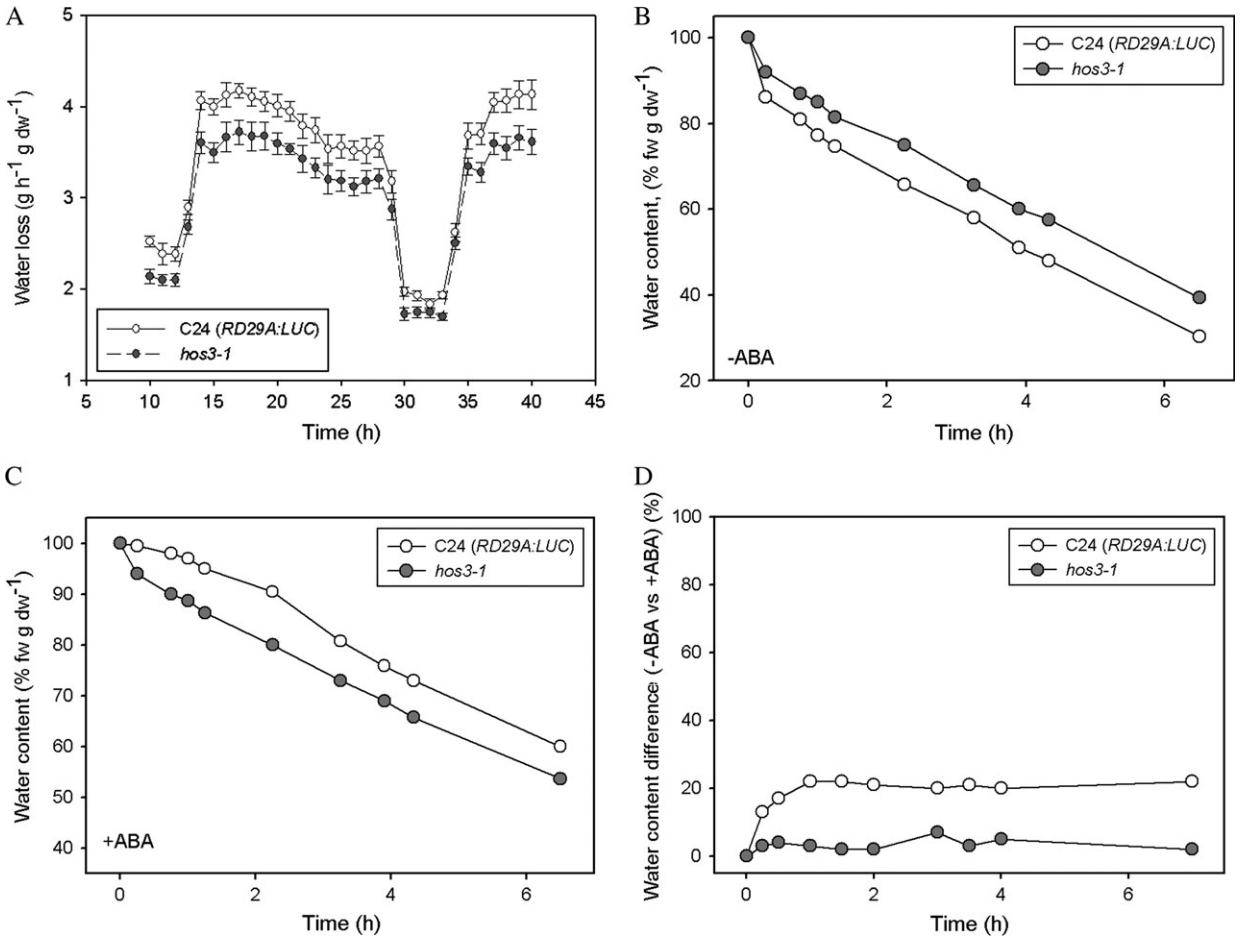

Figure 3. HOS3 Contitutively Regulates Stomatal Aperture Under Well Watered Conditions and Mediates ABA-Induced Stomatal Closure.
(A) Water loss of intact 4-week-old *hos3-1* (closed circles) seedlings was determined gravimetrically and compared with C24 (*RD29:LUC*) wild-type (open circles). Means and standard errors were determined by ANOVA with a confidence interval of $\alpha = 0.05$ for $n = 12$. Error bars represent ± 1 SE.
(B) C24 (*RD29A:LUC*) wild-type (open circles) and *hos3-1* mutant (closed circles) shoots previously untreated or **(C)** treated with ABA (50 μM) were excised for gravimetric water loss determination, expressed as a percent of original fresh weight.
(D) Data from (B) and (C) were plotted to express differential response in C24 (*RD29A:LUC*) wild-type (open circles) or *hos3-1* (closed circles) when treated with ABA.

an unknown protein with homology to CIG30, a 30-kDa cold-induced glycoprotein from *Mus musculus* (Tvrdik et al., 1997). At4g36830 is on BAC clone AP22 starting at position 37071. The T-DNA in *hos3-1* is inserted 513 bp upstream from the translation start codon (Figure 4A). T-DNA LB primer and *HOS3* gene-specific forward primer, used for diagnostic PCR, detected a line with homozygous genotype. PCR products were obtained for several *hos3* lines using this combination of primers while no band was obtained by PCR amplification using forward and reverse gene-specific primers indicating the presence of a T-DNA within At4g36830. Negative controls for both reactions using wild-type lines confirmed these results. A second allele, *hos3-2*, carrying a homozygous insertion was identified from a pool of T-DNA insertional mutants in the Col-0 background. Expression of the *HOS3* transcript was undetectable by RT–PCR in both C24 (*RD29A:LUC*) wild-type and *hos3-1* mutant; expression was detected, however, in the Col-0 ecotype and not in the *hos3-2* mutant allele (Figure 4B). These results suggest expression of *HOS3* may vary among ecotypes and indicates *hos3-2* is a knockout. All T_3 and T_4 lines were homozygous for the *HOS3* mutation, which co-segregated with the CCD phenotype.

hos3-2 Allele Confirms that the Mutation in the *HOS3* Locus is Responsible for the Observed Mutant Phenotypes

Salt sensitivity of the *hos3-2* mutant allele was similar to that of the *hos3-1* allele and showed significant increases in growth of the primary root when treated with NaCl or ABA (Figure 4C and 4D). Average increase in root length of the *hos3-2* mutant was approximately 30% greater than wild-type at moderately

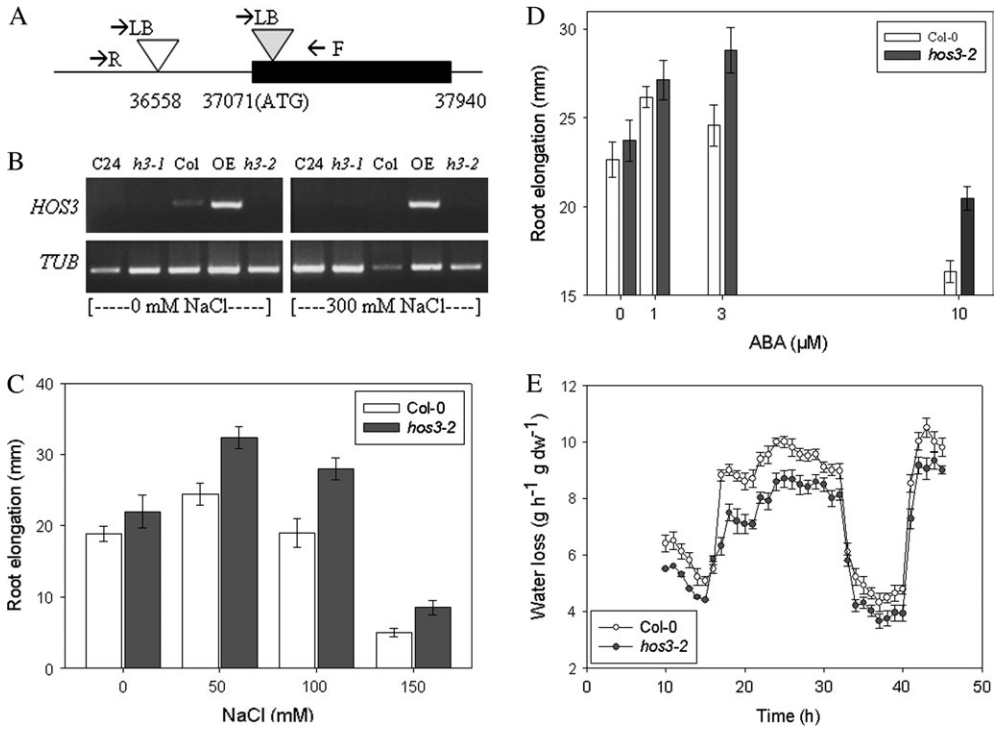

Figure 4. *HOS3* Expression Analysis and Confirmation of the *hos3-2* Phenotypes.

(A) Physical map of T-DNA insertion in the *hos3-1* (open) and *hos3-2* (shaded) mutant alleles (Accession #At4g36830).

(B) Expression of *HOS3* was determined by RT–PCR using *HOS3* gene-specific primers and 1 μg total RNA from C24 (*RD29A:LUC*) (C24), *hos3-1* (*h3-1*), Columbia-0 (Col), Col-0 plants overexpressing HOS3 (OE), and *hos3-2* (*h3-2*). Tubulin (*TUB*) was used as a loading control.

(C) *hos3-2* confirms HOS3 function in osmotic stress response *in vitro* and in constitutive regulation of stomatal aperture under well watered conditions. Root elongation of Col-0 (open bars) and *hos3-2* (closed bars) transferred to media containing NaCl (0, 50, 100, or 150 mM). Means and standard errors were determined using ANOVA with a confidence interval of $\alpha = 0.05$. Error bars represent ± 1 SE.

(D) Root elongation of Col-0 (open bars) or *hos3-2* (closed bars) transferred to media containing ABA (0, 1, 3, or 10 μM).

(E) Water loss of intact 4-week-ld *hos3-2* (closed bars) seedlings was determined gravimetrically and compared with Col-0 (open bars) wild-type. Means and standard errors were determined by ANOVA with a confidence interval of $\alpha = 0.05$ for $n = 12$. Error bars represent ± 1 SE.

high concentrations of NaCl (Figure 4C). Similarly, enhanced root growth in the *hos3-2* allele after ABA treatment resulted in mutant root length that was 20% greater than the Col-0 wild-type primary root length (Figure 4D). Furthermore, stomatal regulation was also impaired as diurnal water loss of intact well watered plants was approximately 13% greater than wild-type, similar to the *hos3-1* allele (Figure 4E). Enhanced root growth upon osmotic stress is consistent with HOS3 functioning as a negative regulator of stress-induced root growth inhibition, or as an inhibitor of ABA, which maintains primary root growth under stress. These results therefore support the idea that *HOS3* functions as a negative regulator of ABA-mediated stress responses and as a constitutive regulator of stomatal opening under favorable conditions.

Wild-Type HOS3 cDNA Expression Restores the Wild-Type Osmotic Stress Sensitivity of *hos3-1*

The function of the wild-type HOS3 allele as a negative regulator of stress responses was confirmed by the restoration of the wild-type *RD29A:LUC* luminescence phenotype in the mutant in response to NaCl treatment (Figure 5A). Further confirmation of this function was seen in the restoration of wild-type root growth upon treatment with NaCl and ABA when a copy of the *HOS3* ORF was expressed in the mutant under the control of the constitutive 35S CaMV promoter (Figure 5B and 5C).

HOS3 Contains Key Features of ELO-Like Proteins

Dissection of the HOS3 protein sequence for key features that may elucidate its function provided evidence to suggest HOS3 could function as an ELO-like protein. Comparison of sequence conservation between the HOS3 predicted protein with the ELO family members, determined using BLASTp software through the NCBI public database, revealed that HOS3 contains a 44% positive match with elongation of fatty acid protein 3 from yeast (*Saccharomyces cerevisiae*), also known as ELO3 or SUR4p. HOS3 does not contain the conserved sequence FLHxYHH, a known part of the ELO catalytic site, and has relatively low sequence similarity to the ELO family of proteins. It does, however conform to the expected topology of the ELO family of proteins. Inconclusive determinations

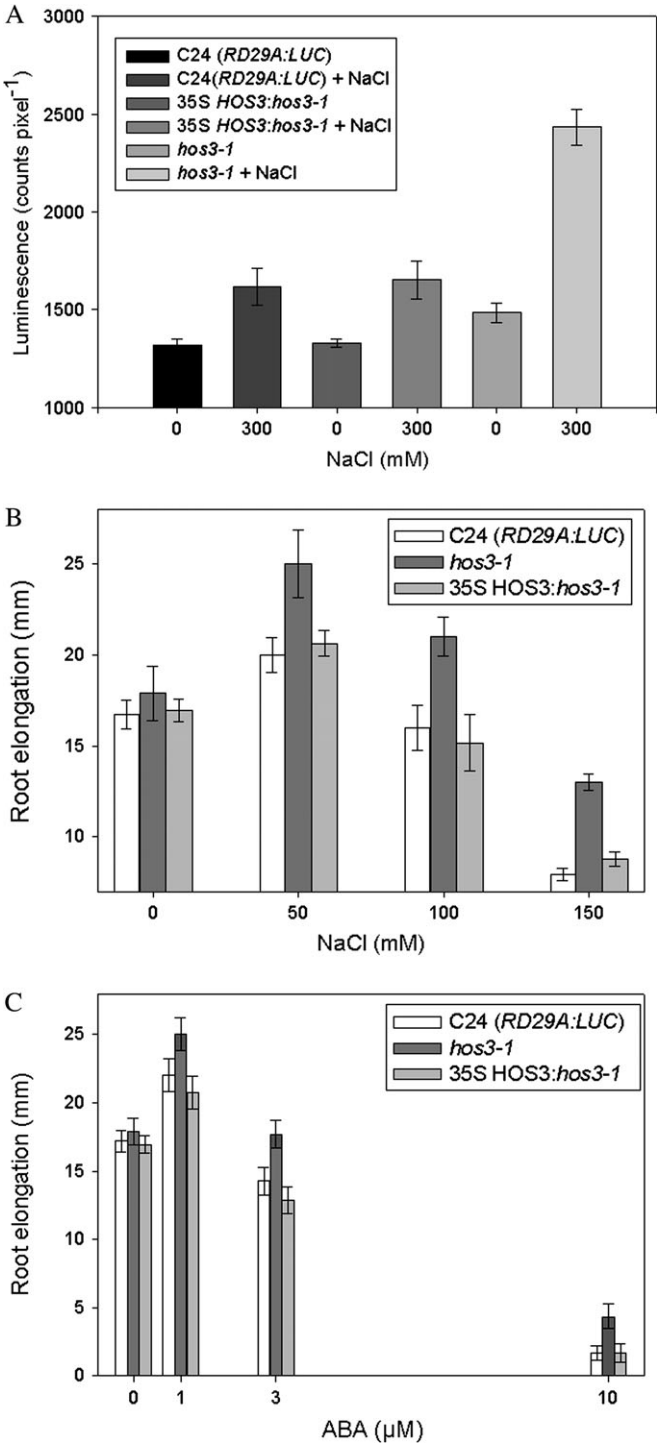

Figure 5. HOS3 Functions as a Negative Regulator of the *RD29A* Stress Response Pathway as 35SCaMV:*HOS3* Restores Wild-Type Sensitivity to NaCl-Stress.

(A) *HOS3* restores wild-type *RD29A:LUC* luminescence to *hos3-1*. Sensitivity to stress was determined by examining changes in luminescence of untreated *hos3-1* (light grey), C24 (*RD29A:LUC*) (dark grey), and 35S *HOS3:hos3-1* (medium grey) plants compared with plants after treatment with 300 mM NaCl. Means and standard errors were determined by ANOVA with a confidence interval of $\alpha = 0.05$. Error bars represent ± 1 SE.

(B) *HOS3* restores wild-type root growth osmotic stress sensitivity to *hos3-1*. *hos3-1* root growth (dark grey bars) is tolerant to all concentrations of NaCl tested (0, 50, 100, and 150 mM) compared with wild-type (open bars), whereas plants expressing the 35SCaMV:*HOS3* (light grey bars) showed restoration of wild-type sensitivity to NaCl. Means and standard errors were determined by ANOVA with a confidence interval of $\alpha = 0.05$. Values are means ± 1 SE.

(C) Root growth of *hos3-1* (dark grey bars) was also compared with growth of plants expressing a 35SCaMV:HOS3 (light grey bars) and wild-type (open bars) after 6 d on media containing ABA (0, 1, 3, and 10 μM).

were made regarding protein localization using PSORT software version 6.4 for prediction of protein localization (data not shown). From this search, it was determined that the probability of targeting this protein to any organelle is low and the known yeast N-terminal sequence, KKxxSTOP to target to the endoplasmic reticulum for fatty acid synthesis, was not present in HOS3. Consistent with a HOS3/ELO relationship, TMpred software used to determine possible transmembrane regions indicated that the strongly preferred model for this protein contains seven transmembrane helices.

HOS3 Functions as an ELO-Like Protein In Planta

Mutation of the *ELO2* and *ELO3* genes from *Saccharomyces cerevisiae* results in increased sensitivity to the antibiotic monensin compared to wild-type (Oh et al., 1997). By transformation of the *elo2* mutant strains with *Arabidopsis HOS3*, almost complete restoration of the wild-type resistance to 100 μg monensin was observed (Figure 6). Further, the monensin-sensitive phenotype of *elo*3 was partially complemented by *HOS3*. Similar evidence of functional complementation was determined directly by comparison of the fatty acid profiles in both plant and yeast.

An indirect pharmacological approach was used to glean clues as to the part of the VLCFA synthesis pathway disrupted by *HOS3-1* mutation. The herbicidal activity of chloroacetamide herbicides, including the S enantiomer of Metolachlor, are known to reduce synthesis of very long chain fatty acids by competitive inhibition of VLCFA-synthase, the enzyme that catalyzes the first step in elongation (Gotz and Boger, 2004). When treated with concentrations of the herbicide greater than 8 μM, primary root growth of the *hos3-1* allele in the C24 (RD29A:LUC) background was 9.4% less than wild-type control (data not shown). Root growth was reduced but was not significantly different from Col-0 wild-type in the *hos3-2* allele (data not shown). Fresh weight of total root was also not significantly different from controls for any of the concentrations tested (data not shown).

Examination of VLCFA methyl ester profiles in plant extracts revealed further evidence of HOS3 function in elongation of VLCFAs. While the concentration of C20:0 FAMES in *hos3-1* was not significantly different from C24(*RD29A:LUC*), mutant plants showed an approximately 15% increase in C22:0 and

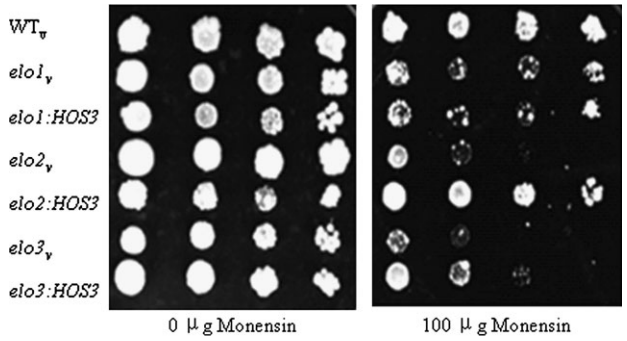

Figure 6. *HOS3* Complements *elo2* and *elo3* Monensin-Sensitive Phenotype.

WT or *elo* mutant yeast cells were transformed with the PYPGE15 vector containing the plant *HOS3* ORF. Serial dilutions of cells were spotted onto selective media containing 0 μg monensin (left panel) or 100 μg monensin (right panel) for 10^4, 10^3, 10^2, or 10^1 cells, respectively, from left to right for each panel shown. Colony growth was compared after 30°C incubation for 4 d. From top to bottom, colonies represent WT vector transformed cells (WT$_v$), *elo2* + vector (*elo2*$_v$), *elo2* + *HOS3* (*elo2*$_v$*:HOS3*), *elo3* + vector (*elo3*$_v$), *elo3* + *HOS* (*elo3*$_v$*:HOS3*).

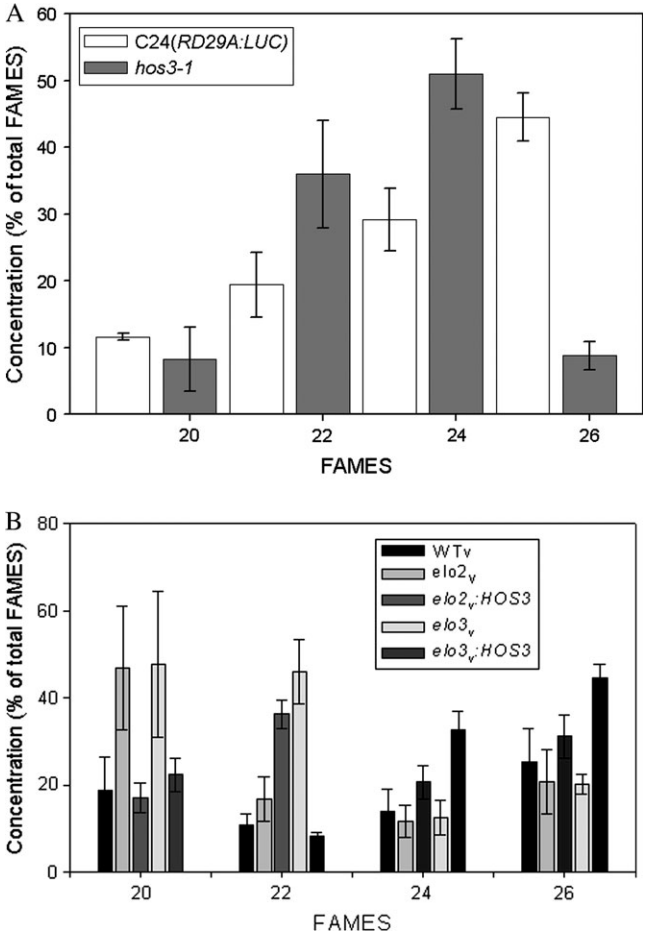

Figure 7. *HOS3* Complements *elo2* and *elo3 In Vivo* and Functions in Synthesis of C26:0 *In Planta*.

VLCFA methyl esters (FAMES) dissolved in hexane were analyzed by gas chromatography with an initial temperature of 80°C, increased at 15°C min^{-1} to 200°C, and then increased at 2°C min^{-1} to 280°C. C20:0, C22:0, C24:0, and C26:0 FAMES were identified by comparison with retention times of known standards run simultaneously. The concentration of individual VLCFA was expressed as a percent of the total C20:0, C22:0, C24:0, and C26:0 FAMES. Values are means ±1 SE.

a 20% increase in C24:0 FAMES compared with wild-type plants, while C26:0 FAMES were reduced more than 35% (Figure 7A). Similarly, VLCFA methyl esters from yeast mutants, complemented with the HOS3 gene from plants, provided additional evidence that suggests HOS3 functionally complements the ELO yeast mutant phenotype. Accumulation of C20:0 VLCFA was evident in *elo2*, and both C20:0 and C22:0 VLCFA accumulated in *elo3* yeast mutants (Figure 7B). HOS3 restored C20:0 to wild-type levels for both *elo2* and *elo3* and also restored C22:0 to wild-type levels in the *elo3* yeast mutant. Interestingly, although C22:0 levels in *elo2* and C24:0 and C26:0 levels in either *elo2* or *elo3* were not significantly different from wild-type, introduction of *HOS3* resulted in significant increases in C22:0 levels in *elo2* as well as significant increases in C24:0 and C26:0 levels in *elo3* (Figure 7B).

DISCUSSION

On the basis of enhanced *RD29A:LUC* luminescence emitted by the *hos3-1* mutant, indicating increased stress sensitivity, it can be inferred that *HOS3* functions as a negative regulator of the *RD29A* stress-responsive pathway (Figure 1). This result lends support to a model in which plant ABA-mediated and NaCl-stress responses would likely increase in the mutant if *HOS3* inhibits ABA. Consistent with this model, other results presented here provide further evidence for HOS3 function in the inhibition of ABA-mediated responses. Specifically, these results support a model in which a defect in *HOS3*, which encodes an elongase-like protein, may confer ABA-hypersensitivity by disrupting VLCFA synthesis and reducing ceramide precursors (Figure 8). ABA is known to mediate stomata closure through S-1-P via GPA1. We propose here that HOS3 functions in synthesis of VLCFA, used for production of ceramides, a potent antagonist for many S-1-P-mediated processes. Disruption of synthesis of VLCFA in the HOS3 mutant leads to the occurrence of many aberrant responses due to the resultant ceramide deficit and, consequently, to an imbalance in the ceramide: S-1-P rheostat.

ABA is required for maintenance of root growth in maize seedlings by suppression of ethylene production (Sharp et al., 2004). ABA is also known to mediate stomatal closure and inhibit seed germination. Whole plant responses of the *hos3-1* mutant displayed several expected alterations in these ABA-mediated responses. Primary root growth on NaCl and

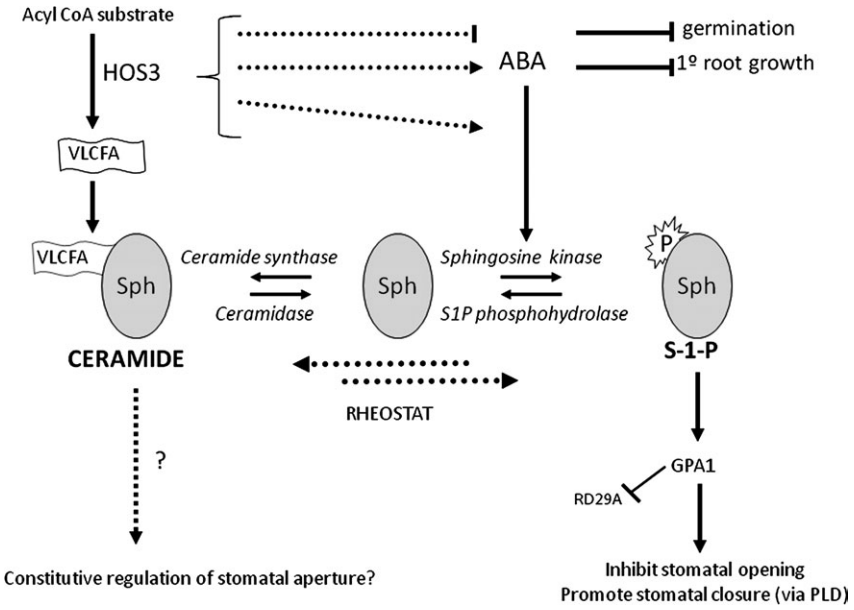

Figure 8. A Proposed Model for the Function of *HOS3* in Constitutive Regulation of Stomatal Aperture and ABA-Induced Stomatal Closure. ABA mediates stomatal closure through sphingosine-1-phosphate (S-1-P), the natural ligand that binds to GPA1 and initiates the signaling cascade that culminates in stomatal closure. HOS3 functions in the synthesis of VLCFA, used for production of ceramides that subsequently function as antagonists for many S-1-P-mediated processes. Disruption of synthesis of VLCFA in the HOS3 mutant leads to the occurrence of many aberrant responses due to the resultant ceramide deficit and, consequently, to an imbalance in the ceramide:S-1-P rheostat.

mannitol osmotic-stress media as well as growth on ABA media (Figure 2A and 2B) was enhanced in *hos3-1*. Furthermore, *hos3-2* also resulted in similarly impaired stress responses affecting root growth under NaCl stress and ABA-treatment (Figure 4C and 4D). Other ABA-mediated responses were also affected by the mutation, including reduced germination (Figure 2C) and enhanced ABA-mediated stomatal closure (Figure 3D), lending additional credence to the hypothesis that HOS3 functions as a negative regulator of ABA-dependent processes. Furthermore, both *hos3-1* and *hos3-2* mutant alleles displayed reduced water loss under non-stress conditions (Figures 3A and 4E), which may reflect complex regulation of stomatal behavior arising from the interactions of HOS3, far upstream of other known stomatal effectors.

Under both desiccation stress and well watered conditions, a dynamic balance of both positive and negative regulators of stomatal aperture is necessary to ensure optimal CO_2 uptake while limiting transpirational water loss. Under favorable conditions, this balance is achieved, in part, by negative regulation of stress responses to promote stomatal opening and to maximize uptake of CO_2. Reduced transpiration in both *hos3* alleles is consistent with HOS3 function in inhibiting ABA-mediated stomatal closure. Further, the reduced effect of ABA treatment on water loss in the *hos3-1* mutant suggests that the stomata of mutant plants were almost completely closed prior to ABA treatment. Complementation of the CCD luminescence phenotype (Figure 5A) and the NaCl and ABA root growth phenotypes (Figure 5B and 5C) provides strong evidence that HOS3 functions as a negative regulator of ABA-mediated stress responses and, through its role in synthesis of VLCFA, may function in stomatal regulation by creating an imbalance in the ceramide:S-1-P rheostat.

Results shown here provide bioinformatics, yeast complementation (Figure 6), biochemical (Figure 7A and 7B), and pharmacological evidence to support the idea that the *HOS3* gene product participates in synthesis of very long chain fatty acids similar to the *ELO2* and *ELO3* gene products from *Saccharomyces cerevisea* (Oh et al., 1997). ELO2 and ELO3 act downstream of ELO1 and catalyze with high efficiency the elongation of C22:0 fatty acids to VLCFA of 24 and 26 carbons, respectively (Oh et al., 1997). However, both have broad and varied substrate specificity for elongation of C18:0 to C26:0 VLCFA (Dunn et al., 2004). VLCFA are required for the subsequent synthesis of ceramide and the three types of inositol-containing sphingolipids in yeast (reviewed by Lester and Dickson, 1993). ELO2 and ELO3 appear to serve partially overlapping functions, as ceramide and inositol sphingolipid synthesis were not completely abolished by the disruption of either gene, and mutations in each individual gene had few phenotypic effects upon cell growth (Oh et al., 1997). As predicted, introduction of the *HOS3* ORF into *elo2* and *elo3* mutants complemented their antibiotic sensitivity as determined from almost complete restoration of wild-type growth in *elo2* and improved growth in *elo3* on 100 μM monensin (Figure 6). Monensin resistance of the two complemented yeast mutants suggests the *HOS3* gene product may serve a similarly redundant function in plants with primary function in synthesis of 24:0 carbon VLCF acyl chains from 22:0 substrate, like ELO2, and with overlapping substrate specificity for 24:0 chain lengths, like ELO3. In yeast, disruption of both *ELO2* and *ELO3* genes resulted in a loss of sphingolipid synthesis and had a lethal phenotype in yeast (Oh et al., 1997). These results provide stimulus for future research to investigate the possibility that an analogous pairing may exist in plants.

Biochemical characterization of VLCFA in plants confirmed our conclusions based on the observed restoration of monensin resistance in both *elo2* and *elo3* when complemented with *HOS3*. Accumulation of C22:0 and C24:0 levels, along with

a five-fold reduction in C26:0 compared with wild-type plants, indicates that HOS3 functions in synthesis of both C24:0 and C26:0 (Figure 7A). Failure to accumulate C20:0 in *hos3-1*, as was evident in *elo2* and *elo3*, indicates that the catalytic specificity of HOS3 differs somewhat from that of ELO2 and ELO3. Accumulation of C20:0 in *elo2* and *elo3* confirmed results previously published (Oh et al., 1997) that indicated overlapping catalytic specificity of ELO2 and ELO3 (Figure 7B). Similarly, *HOS3* restored high C20:0 levels to wild-type levels in both *elo2* and *elo3* (Figure 7B). Furthermore, *elo2:HOS3* showed significant increases in C22:0, which reiterates the importance of HOS3 in conversion of C20:0 to C22:0 (Figure 7B). Accumulation of C22:0 in *elo3*, while *elo2* maintained wild-type levels of this VLCFA, confirms ELO3 has higher efficiency in converting C22:0 to C24:0 (Figure 7B). In plants, it was expected that *HOS3* would complement these *elo2* and *elo3* phenotypes in conversion of C22:0 to C24:0 and conversion of C24:0 to C26:0. In support of this hypothesis, *HOS3* restored C22:0 levels in *elo3* to wild-type levels—a result suggesting that C22:0 is used as substrate for synthesis of C24:0 (Figure 7B). Furthermore, C24:0 levels in *elo3:HOS3* were significantly higher than those in *elo3* and wild-type (Figure 7B), indicating that HOS3 functions in converting C24:0 to C26:0—a conclusion also suggested by low C26:0 levels in planta (Figure 7A).

Combined, *elo* yeast mutant complementation and altered stress responses measured in planta lend support to a model in which VLCFA functions in abiotic stress signaling (Sperling and Heinz, 2003). There is abundant evidence in current literature to support several possible mechanisms for this conserved relationship in both yeast and plant systems (Leonard et al., 2004). In general, disruption of VLCFA synthesis in yeast reduces sphingolipid pools and leads to subsequent decreases in key sphingolipid signaling compounds (Oh et al., 1997). Sphingolipids have been thoroughly investigated and repeatedly shown to serve in signaling roles in plant growth and development and in response to stress. Consequently, because VLCFA are critical for the sphingolipid signaling pathway, defects in synthesis of VLCFA should lead to phenotypic disruptions in sphingolipid-mediated processes, including growth, development, and normal response to abiotic and biotic stresses (Van Brocklyn et al., 1998; Sperling and Heinz, 2003; Worrall et al., 2003; Zheng et al., 2005; Qin et al., 2007; Raffaele et al., 2008). Among the spingolipids, membrane-localized ceramide has been found to play essential roles in the induction of programmed cell death in yeast cells in response to adverse stresses (Taha et al., 2006). Ceramide-1-phosphate and ceramide can be interconverted in the cells, and ceramide serves as substrate to generate sphingosine-1-phosphate (S-1-P). S-1-P is known to mediate ABA responses of stomata in *Arabidopsis* via the heterotrimeric G-protein subunit encoded by *GPA1* (Coursol et al., 2003). Loss of function in the heterotrimeric G-protein alpha and beta subunits *GPA1* and *AGB1,* of *Arabidopsis* abrogates the inhibitory effect of ABA on inward K^+ (K_{in}) currents and stomatal opening (Wang et al., 2001; Coursol et al., 2003; Fan et al., 2008). S-1-P accumulates in response to drought stress, stimulates calcium oscillations necessary for guard cell closure, and functions in the signal transduction pathway leading from ABA to stomatal closure in *Commelina communis* leaves (Ng et al., 2001). Importantly, the heterotrimeric G-protein-based pathway not only functions in guard cells, but also plays critical roles in glucose sensing, cell division, and plant development (Ullah et al., 2001; Chen et al., 2004; Chen et al., 2006; Huang et al., 2006; Pandey et al., 2006; Johnston et al., 2007).

HOS3 functions antagonistically to ABA in regulating stomatal closure and seed germination (Figures 2C, 3A–3D, and 4E). The mechanism by which HOS3 inhibits ABA-mediated responses, accounting for the variety of ABA-hypersensitive responses observed in the *hos3* mutants, may involve disrupted regulation of the S-1-P antagonist, ceramide (Figure 8). The concept of a rheostat that regulates the balance of intracellular S-1-P and ceramide and the consequent regulation of opposing signaling pathways is both plausible and useful in explaining the effects we have observed (Spiegel and Milstien, 2000, 2002; Kobayashi and Nagiec, 2003). The sphingolipid rheostat, consisting of a set of enzymes that regulate the levels of ceramide, is evolutionarily conserved in all eukaryotes (Kobayashi and Nagiec, 2003). This rheostat also plays a role in regulation of stress responses of yeast cells (Cuvillier et al., 1996; Mandala et al., 1998; Jenkins and Hannun, 2001; Spiegel and Milstien, 2002) and is strongly dependent on the supply of C26:0 CoA (Kobayashi and Nagiec, 2003).

Generally, the modest phenotypes and absence of obvious growth defects observed in *hos3-1* and *hos3-2* and also reported for *elo2* and *elo3* (Oh et al., 1997) suggest that redundant pathways leading to synthesis of VLCFA also likely exist in plants. In yeast, it is clear that there are alternate paths in secretion to the cell surface that are regulated by v-SNARE bypass mutants (VBM), known alleles of the *ELO2* and *ELO3* genes (David et al., 1998). v*bm*/*elo* mutants were shown to bypass the usual v-SNARE coupling mechanism for vesicle docking with corresponding membrane-localized t-SNARE protein (David et al., 1998). The ability of the *vbm* mutants to partially suppress the defect in exocytosis, in the absence of the normal v-SNARE, *snc*, indicate that v-SNARES are not essential for secretion, but instead contribute to increasing efficiency of vesicle docking and fusion and suggest that an alternate or secondary route exists that facilitates vesicle trafficking to the membrane (David et al., 1998). David et al. (1998) proposed that, whereas proteins essential for growth reach the cell surface by either route, nonessential cargo is more specifically regulated by sphingolipids. This idea is substantiated for both the yeast and plant systems by the robust growth phenotypes for both the *vbm* and *hos3* mutants.

Data presented here provide evidence that the plant gene *HOS3* functions in synthesis of VLCFA and functions as a negative regulator of ABA-mediated stress responses possibly through the action of antagonistic signaling pathways mediated through either S-1-P or ceramide. Yet, several critical questions remain unanswered, especially with regard to the

identity of specific downstream lipid mediators that may be affected by defects in this component of VLCFA synthesis. Further, elucidation of the interaction of *HOS3* with other *Arabidopsis* homologs functioning in v-SNARE-mediated secretion would deepen our understanding of the role of sphingolipids in abiotic stress signaling networks.

METHODS

Plant Material

Activation T-DNA-tagged (Weigel et al., 2000) mutations were generated by *Agrobacterium tumefaciens*-mediated transformation of inflorescences (Clough and Bent, 1998). *Arabidopsis thaliana* (C24 ecotype) expressing the *RD29A:LUC* transgene (referred to as the wild-type) with altered abiotic stress-responsiveness were selected based on alterations in their expression of the luciferase transgene, as described (Ishitani et al., 1997). T_2 seeds were plated on ½ × MS (Murashige and Skoog) salt (JRH Biosciences, Lenex, KS) based media with 0.8% agar. Seeds were germinated and grown at 22°C under continuous white light. One-week-old seedlings were screened for altered *RD29A:LUC* expression by visualizing luminescence in response to 300 mM NaCl, 100 μM ABA or low temperature using a thermoelectrically cooled charge-coupled device (CCD) camera. Prior to visualizing luminescence, plants were sprayed with 1 mM luciferin in 0.01% Tween 20 solution and incubated in the dark at room temperature for 5 min (Xiong et al., 1999). Images were acquired with a 5-min exposure time before quantifying the luminescence intensity of each seedling with Win-View software (Princeton Instruments, Trenton, NJ).

The *hos3-2* mutant allele (Salk_064585), designated *hos3-2*, derived from the Salk institute in the Columbia-0 background was selected for homozygous genotype by diagnostic PCR using HOS3 specific primers (described under genetic analysis) (Alonso et al., 2003).

Plant Growth Conditions

For *in-vivo* experiments, T_3 plants with homozygous phenotype on soil were selected and grown for all experiments. Seeds were sown in moistened Scotts MetroMix 360. After being stratified at 4°C for 5 d, flats were germinated and grown in Perceival™ growth chambers under 16-h photoperiod with cool white fluorescent lighting at 100 μmol $m^{-} s^{-1}$. For growth experiments, plants were transplanted into Turface® calcined clay after 10 d and sub-irrigated with 100 ppm N. Daytime temperature was maintained at 21°C and night temperature was set to 19°C.

To detect *RD29A:LUC* luminescence, surface sterilized T_3 seeds were plated as described above for mutant screening. Seedlings grown *in vitro* were treated with ABA (100 μM (±)-*cis*,*trans*-ABA in 0.01% Tween20) by spraying uniformly on the leaves of 7-day-old seedlings. Plates were then incubated at room temperature under cool-white light for 4 h for both luminescence imaging and RNA analysis. Alternatively, for NaCl treatment, seedlings on MS plates were transferred to filter paper saturated with 300 mM NaCl in deoinized water and incubated for 4 h.

For *in-vitro* root growth experiments, surface sterilized seeds were sown onto germination ½ × MS media with 1.2% agar, pH 5.7. Six-day-old seedlings were transferred onto basal media containing NaCl (0, 50, 100, or 150 mM) or mannitol (0, 200, 300, or 400 mM). The position of the primary root tip was marked on the plate at the time of transfer and growth after six additional days was determined. s*tt*3 was used as a positive control for NaCl and mannitol root growth (Koiwa et al., 2003). Root growth on ABA (0, 1, 3, 10, and 30 μM) was measured after 4 d. Means and standard errors were determined by ANOVA with a confidence interval of $\alpha = 0.05$ for $n = 50$ samples. Herbicide-sensitivity was tested by growing seedlings on R, S Metolachlor (0, 2, 4, 8, 16, or 32 μM). Position of the primary root tip was noted after 5 d, and its elongation was measured after an additional 7 d. Means and standard errors for 25 plants were determined using ANOVA with a confidence interval of $\alpha = 0.05$.

For germination tests, seeds of T_3 mutant and wild-type C24 (*RD29A:LUC*) were sterilized and stratified for 5 d at 4°C. Seeds were then plated onto ½ × MS media with 1.0% agar containing ABA (0, 0.1, 0.3, 0.6, or 0.9 μM). Plates were sealed with parafilm and left under long day conditions to germinate. Percent germination was determined after 9 d relative to the number of seeds germinating on 0 μM ABA.

Genetic Analysis of hos3 T-DNA Insertion Alleles

The genomic sequence flanking T-DNA in *hos3-1* was determined using the thermal asymmetric interlaced–PCR (TAIL–PCR) method as described previously (Koiwa et al., 2003). To isolate plants containing homozygous T-DNA insertions, gene-specific primers were designed around the insertion, which was 513 bp upstream of the translational start codon of the accession At4g36830 on BAC clone AP22 (starting at position 37071). Genotype was determined by diagnostic PCR performed using primer F1 (5′gtaagttcaccgtccaagtctcc3′), R1 (5′ctccaacggaatccgacgatg3′) and LB1 (5′gtagatgrccgcgcagcgtatta3′) for the *hos3-1* allele and F1, R1 with the Salk LBa1 primer (5′ tggttcacgtagtgggccatcg 3′) for the *hos3-2* allele. The gene-specific reverse primer was used for diagnostic PCR along with the T-DNA left border primer to identify plants with homozygous genotype.

Molecular Characterization

Seedlings were grown and treated as described for CCD experiments before being harvested and stored at –80°C for RNA analysis. RNA was isolated from 12-day-old seedlings grown in ½ × MS medium (pH 5.7) using the TRIzol Reagent (INvitrogen, Carlsbad, CA). First-strand cDNA was synthesized using the SuperScript III two-step kit (INvitrogen Corp. Carlsbad, CA) with 1 μg of total RNA according to the protocol recommended in the manual. The RT–PCR reaction was carried out using the

HOS3 gene-specific primers described under the genetic analysis heading in the Methods section. Expression of *RD29A* was determined using gene-specific primers including F (5′ cccggatccttttctgatatggttgcc 3′) and R (5′gccctc gagccgaacaatttattaacc 3′) and Tubulin loading control was amplified using F (5′cctgataacttcgtctttgg 3′) and R (5′gtgaactccatctcgtcat 3′).

Bioinformatics

NCBI BLASTp software was used to identify homologous proteins for the predicted hos3 protein (Accession #CAB 80349.1). PSORT was used to predict localization. Conserved domains were searched using the citing CD (Marchler-Bauer et al., 2003) web tool through the NCBI database. TMpred software was used to predict protein topology.

Stomatal Aperture Assays and Stomatal Water Loss

Excised shoots from 18 well watered 4-week-old plants were placed on three balances each for wild-type, *hos3-1*, and *hos3-2* mutant lines, respectively. Weight was logged in 10-min intervals from each balance by computer using Software wedge v1.2 (TAL Technologies, Inc., Philadelphia, PA). Water loss was then standardized relative to total shoot dry weight and presented as a percent of shoot dry weight. Means and standard errors were calculated (n = 18) using ANOVA (α = 0.05). Intact plants were used for quantitation of diurnal water loss rates. Diurnal whole plant water loss was determined gravimetrically using pots containing 4-week-old seedlings that were sealed with clear plastic wrap to prevent water loss from the soil. A total of 12 seedlings for each line tested were then placed on a balance and weights were logged in 1-h intervals for 48 h. For ABA treatment, abaxial and adaxial leaf surfaces were sprayed with ABA (50 μM solution (0.01% Tween 20) daily and allowed to dry before weights were recorded. Rate of water loss was calculated on the basis of shoot dry weight and recorded as grams of water lost per hour per gram of dry weight. Means and standard errors were calculated using ANOVA (α = 0.05). Measurements of stomatal aperture were performed for 4-week-old seedlings, treated either by spraying with a 100-μM ABA solution on all plant surfaces or by removing the plant from the pot, washing the roots free of soil and allowing the plant to dry 2 h before abaxial epidermal peels were taken. Peels were photographed under light microscope at 400× magnification, and digital images obtained in this way were analyzed using SCION image© for Windows. Guard cell aperture measurements represent the total aperture at 400× magnification. Control plants were wells watered plants sprayed with distilled water containing 0.01% Tween 20. Values presented are the means and standard errors of 40 samples determined using ANOVA with a confidence interval of α = 0.05.

Yeast Mutant Complementation

WT or *elo* mutant yeast cells were transformed with the PYPGE15 vector containing the plant *HOS3* ORF using the rapid PLATE transformation method (Elble, 1992). *elo* mutant strains and PYPGE15 vector were histidine and uracil autotropic, respectively. Transformed cells were selected in Selective Complete (SC) media lacking either uracil or both histidine and uracil for transformed wild-type or *elo* mutants, respectively. Cells were then plated on their respective selective plate media, and presence of the *HOS3* gene was confirmed in individual colonies by colony PCR using *HOS3* gene-specific primers described above. Positive transformants were cultured in selective liquid culture from which an aliquot containing 1×10^4 cells was reserved for serial dilutions equal to 10 000, 1000, 100, or 10 cells and spotted onto selective media plates containing 100 μM monensin. Growth of colonies was compared following incubation at 30°C for 4 d.

Genetic Complementation

Two different genomic DNA fragments containing the *HOS3* open reading frame were digested from the bacterial artificial chromosome AP22 with Sst1 and Xba1 restriction enzymes. *hos3-1* mutant plants were transformed by *Agrobacterium tumefaciens*-mediated transformation of inflorescence with pCambia 99-1 cloning vector (*Sst*1/*Xba*1) containing the native *HOS3* ORF under the control of the 35S promoter and the hygromycin selectable marker. Positive transformants were selected on full-strength MS media containing 35 mg L^{-1} hygromycin. Survivors were rescued to soil, self-fertilized and the resulting T_1 seeds were plated onto selection media again to identify lines homozygous for the transgene. *HOS3* overexpression lines were generated in the identical manner with the native *HOS3* gene under the control of the 35S CaMV promoter and the hygromycin selectable marker. The progeny of segregating T_2 populations derived from hygromycin-resistant T_1 lines (plants obtained from seed of plants directly after floral transformation) were evaluated for hygromycin resistance on 35 mg L^{-1} hygromycin.

Lipid Extraction and Fatty Acid Analysis

Total lipids were extracted from 0.5 g of fresh, frozen plant leaf material or 1.5 mg of dry lipid extract from yeast cells as described previously (Swan and Watson, 1997). Lipids were transmethylated with a 10% solution of BF_3 by heating at 80°C for 15 min and then extracting three times in 0.5 ml hexane. Fatty acid methyl esters (FAMES) were derivitized with 50 μl BSTFA and incubated at 70°C for 30 min. BF_3 was dried off under a stream of N_2 gas and FAMES were dissolved into hexane for analysis by gas chromatography. C20:0, C22:0, C24:0, and C26:0 FAMES were identified by comparison with retention times of known standards run simultaneously. A Hewlett-Packard 5890 series II gas chromatograph (GC) equipped with a flame ionization detector was equipped with a 12-m, 0.2-mm HP-1 capillary column with helium as the carrier gas. The GC was programmed with an initial temperature of 80°C and increased at 15°C min^{-1} to 200°C, then increased at 2°C min^{-1} to 280°C. The concentrations of individual VLCFA were expressed as a percent of the total C20:0, C22:0, C24:0, and C26:0 FAMES.

FUNDING

This research was supported by United States Department of Agriculture National Needs Grant 98-38420-5847 to R.J.J., by the National Science Foundation Plant Genome Award DBI-98-13360 to R.A.B., and by the One Hundred Young Talents Program of Chinese Academy of Sciences to X.L.

ACKNOWLEDGMENTS

We are grateful to our lab members who gave us support in our research. No conflict of interest declared.

REFERENCES

Alonso, J.M., et al. (2003). Genome-wide insertional mutagenesis of *Arabidopsis thaliana*. Science. **301,** 653–657.

Blacklock, B.J., and Jaworski, J.G. (2006). Substrate specificity of *Arabidopsis* 3-ketoacyl-CoA synthases. Biochem. Biophys. Res. Comm. **346,** 583–590.

Brown, D.A., and London, E. (2000). Structure and function of sphingolipid- and cholesterol-rich membrane rafts. J. Biol. Chem. **275,** 17221–17224.

Chen, J.G., Gao, Y., and Jones, A.M. (2006). Differential roles of *Arabidopsis* heterotrimeric G-protein subunits in modulating cell division in roots. Plant Physiol. **141,** 887–897.

Chen, Y.-L., Huang, R., Xiao, Y.-M., Lu, P., Chen, J., and Wang, X.-C. (2004). Extracellular calmodulin-induced stomatal closure is mediated by heterotrimeric G protein and H_2O_2. Plant Physiol. **136,** 4096–4103.

Clough, S.J., and Bent, A.F. (1998). Floral dip: a simplified method for *Agrobacterium*-mediated transformation of *Arabidopsis thaliana*. Plant J. **16,** 735–743.

Coursol, S., Fan, L.-M., Le Stunff, H., Spiegel, S., Gilroy, S., and Assmann, S.M. (2003). Sphingolipid signalling in *Arabidopsis* guard cells involves heterotrimeric G proteins. Nature. **423,** 651–654.

Coursol, S., LeStunff, H., Lynch, D.V., Gilroy, S., Assmann, S.M., and Spiegel, S. (2005). *Arabidopsis* sphingosine kinase and the effects of phytosphingosine-1-phospate on stomatal aperture. Plant Phys. **137,** 724–737.

Cuvillier, O., Pirianov, G., Kleuser, B., Vanek, P.G., Coso, O.A., Gutkind, J.S., and Spiegel, S. (1996). Suppression of ceramide-mediated programmed cell death by sphingosine-1 phosphate. Nature. **381,** 800–803.

David, D., Sundarababu, S., and Gerst, J. (1998). Involvement of long chain fatty acid elongation in the trafficking of secretory vesicles in yeast. J. Cell Biol. **143,** 1167–1182.

Dietrich, C.R., Perera, A.D.N., Yandeau-Nelson, M.D., Meeley, R.B., Nikolau, B.J., and Schnable, P.S. (2005). Characterization of two *GL8* paralogs reveals that the 3-ketoacyl reductase component of fatty acid elongase is essential for maize (*Zea mays* L.) development. Plant J. **42,** 844–61.

Dunn, T.M., Lynch, D.V., Michaelson, L.V., and Napier, J.A. (2004). A post-genomic approach to understanding sphingolipid metabolism in *Arabidopsis thaliana*. Ann. Bot. **934,** 483–497.

Elble, R. (1992). A simple and efficient procedure for transformation of yeasts. Biotechniques. **13,** 18–20.

Fan, L.M., Zhang, W., Chen, G., Taylor, J.P., Jones, A.M., and Assmann, S.M. (2008). Abscisic acid regulation of guard-cell K+ and anion channels in Gβ- and RGS-deficient *Arabidopsis* lines. Proc. Natl Acad. Sci. U S A. **105,** 8476–8481.

Gotz, T., and Boger, P. (2004). The very-long-chain fatty acid synthase is inhibited by chloroacetamides. Naturforsch. **59,** 549–553.

Gray, J.E., Holroyd, G.H., van der Lee, F.M., Bahrami, A.R., Sijmons, P.C., Woodward, F.I., Schuch, W., and Hetherington, A.M. (2000). The *HIC* signaling pathway links CO_2 perception to stomatal development. Nature. **408,** 713–716.

Hakomori, S., and Igarashi, Y. (1995). Functional-role of glycosphingolipids in cell recognition and signaling. J. Biochem. **118,** 1091–1103.

Holthuis, J.C.M., Pomorski, T., Raggers, R.J., Sprong, H., and Van Meer, G. (2001). The organizing potential of sphingolipids in intracellular membrane transport. Physiol. Rev. **81,** 1689–1723.

Huang, J., Taylor, J.P., Chen, J.G., Uhrig, J.F., Schnell, D.J., Nakagawa, T., Korth, K.L., and Jones, A.M. (2006). The plastid protein THYLAKOID FORMATION1 and the plasma membrane G-protein GPA1 interact in a novel sugar-signaling mechanism in *Arabidopsis*. Plant Cell. **18,** 1226–1238.

Ishitani, M., Xiong, L.M., Stevenson, B., and Zhu, J.-K. (1997). Genetic analysis of osmotic and cold stress signal transduction in *Arabidopsis:* interactions and convergence of abscisic acid-dependent and abscisic acid-independent pathways. Plant Cell. **9,** 1935–1949.

Jenkins, G.M., and Hannun, Y.A. (2001). Role for de novo sphingoid base biosynthesis in the heat-induced transient cell cycle arrest of Saccharomyces cerevisiae. J. Biol. Chem. **276,** 8574–8581.

Johnston, C.A., Taylor, J.P., Gao, Y., Kimple, A.J., Grigston, J.C., Chen, J.G., Siderovski, D.P., Jones, A.M., and Willard, F.S. (2007). GTPase acceleration as the rate-limiting step in *Arabidopsis* G protein-coupled sugar signaling. Proc. Natl Acad. Sci. U S A. **104,** 17317–17322.

Kobayashi, S.D., and Nagiec, M.M. (2003). Ceramide/long-chain base phosphate rheostat in *Saccharomyces cerevisiae*: regulation of ceramide synthesis by Elo3p and Cka2p. Eukaryot. Cell. **2,** 284–294.

Koiwa, H., et al. (2003). The STT3a subunit isoform of the *Arabidopsis* oligosaccharyltransferase controls adaptive responses to salt/osmotic stress. Plant Cell. **15,** 2273–2284.

Kolesnick, R.N., and Kronke, M. (1998). Regulation of ceramide production and apoptosis. Annu. Rev. Physiol. **60,** 643–665.

Leonard, A.E., Pereira, S.L., Sprecher, H., and Huang, Y.-S. (2004). Elongation of long-chain fatty acids. Progress in Lipid Research. **43,** 36–54.

Lester, R.L., and Dickson, R.C. (1993). Sphingolipids with inositol-phosphate-containing head groups. Adv. Lipid Res. **26,** 253–274.

Lester, R.L., Wells, G.B., Oxford, G., and Dickson, R.C. (1993). Mutant strains of Saccharomyces cerevisieae lacking sphingolipids synthesize novel inositiol glycerophospholipids that mimic sphingolipid structures. J. Biol. Chem. **268,** 845–856.

Liang, H., Yao, N., Song, J.T., Luo, S., Lu, H., and Greenberg, J.T. (2003). Ceramides modulate programmed cell death in plants. Genes Dev. **17,** 2636–2641.

Mandala, S.M., Thornton, R., Tu, Z., Kurtz, M.B., Nickels, J., Broach, J., Menzeleev, R., and Spiegel, S. (1998). Sphingoid base 1-phosphate phosphatase: a key regulator of sphingolipid metabolism and stress response. Proc. Natl Acad. Sci. U S A. **95,** 150–155.

Marchler-Bauer, A., et al. (2003). CDD: a curated Entrez database of conserved domain alignments. Nucleic Acids Res. **31,** 383–387.

Merrill, A.H. (2002). De novo sphingolipid biosynthesis: a necessary, but dangerous, pathway. J. Biol. Chem. **277,** 25843–25846.

Millar, A.A., Clemens, S., Zachgo, S., Giblin, E.M., Taylor, D.C., and Kunst, L. (1999). CUT1, an *Arabidopsis* gene required for cuticular wax biosynthesis and pollen fertility, encodes a very-long-chain fatty acid condensing enzyme. Plant Cell. **11,** 825–838.

Ng, C.K.-Y., Carr, K., McAinsh, M.R., Powell, B., and Hetherington, A.M. (2001). Drought-induced guard cell signal transduction involves sphingosine-1-phosphate. Nature. **410,** 596–599.

Oh, C.-S., Toke, D.A., Mandala, S., and Martin, C.E. (1997). *ELO2* and *ELO3*, homologues of the *Saccharomyces cerevisea ELO1* gene, function in fatty acid elongation and are required for sphingolipid formation. J. Biol. Chem. **272,** 17376–17384.

Pandey, S., Chen, J.G., Jones, A.M., and Assmann, S.M. (2006). G-protein complex mutants are hypersensitive to abscisic acid regulation of germination and postgermination development. Plant Physiol. **141,** 243–256.

Paul, S., Gable, K., Beaudoin, F., Cahoon, E., Jaworski, J., Napier, J.A., and Dunn, T.M. (2006). Members of the *Arabidopsis* FAE1-like 3-ketoacyl-CoA synthase gene family substitute for the elop proteins of Saccharomyces cerevisiae. J. Biol. Chem. **281,** 9018–9029.

Pruitt, R.E., Vielle-Calzada, J.-P., Ploense, S.E., Grossniklaus, U., and Lolle, S.J. (2000). FIDDLEHEAD, a gene required to suppress epidermal cell interactions in *Arabidopsis*, encodes a putative lipid biosynthetic enzyme. Proc. Natl Acad. Sci. U S A. **97,** 1311–1316.

Pyne, S., and Pyne, N.J. (2000). Sphingosine 1-phosphate signalling in mammalian cells. Biochem. J. **349,** 385–402.

Qin, Y.M., Hu, C.Y., Pang, Y., Kastaniotis, A.J., Hiltunen, J.K., and Zhu, Y.X. (2007). Saturated very-long-chain fatty acids promote cotton fiber and *Arabidopsis* cell elongation by activating ethylene biosynthesis. Plant Cell. **19,** 3692–3704.

Raffaele, S., Vailleau, F., Léger, A., Joubès, J., Miersch, O., Huard, C., Blée, E., Mongrand, E., Domergue, F., and Roby, D. (2008). A MYB transcription factor regulates very-long-chain fatty acid biosynthesis for activation of the hypersensitive cell death response in *Arabidopsis*. Plant Cell. **20,** 752–767.

Sharp, R.E., Poroyko, V., Hejlek, L.G., Spollen, W.G., Springer, G.K., Bohnert, H.J., and Nguyen, H.T. (2004). Root growth maintenance during water deficits: physiology to functional genomics. J. Exp. Bot. **55,** 2343–2351.

Sperling, P., and Heinz, E. (2003). Plant sphingolipids: structural diversity, biosynthesis, first genes and functions. Biochim. Biophys Acta. **1632,** 1–15.

Spiegel, S., and Milstien, S. (2000). Sphingosine-1-phosphate: signaling inside and out. FEBS Lett. **476,** 55–57.

Spiegel, S., and Milstien, S. (2002). Sphingosine 1-phosphate, a key cell signaling molecule. J. Biol. Chem. **277,** 25851–25854.

Swan, T.M., and Watson, K. (1997). Membrane fatty acid composition and membrane fluidity as parameters of stress tolerance in yeast. Can. J. Microbiol. **43,** 70–77.

Taha, T.A., Mullen, T.D., and Obeid, L.M. (2006). A house divided: ceramide, sphingosine, and sphingosine-1-phosphate in programmed cell death. Biochim. Biophys. Acta. **1758,** 2027–2036.

Tehlivets, O., Scheuringer, K., and Kohlwein, S.D. (2007). Fatty acid synthesis and elongation in yeast. Biochem. Biophys Acta. **1171,** 255–270.

Townley, H.E., McDonald, K., Jenkins, G.I., Knight, M.R., and Leaver, C.J. (2005). Ceramides induce programmed cell death in *Arabidopsis* cells in a calcium-dependent manner. Biol. Chem. **386,** 161–166.

Tvrdik, P., Asadi, A., Kozak, L.P., Nedergaard, J., Cannon, B., and Jacobsson, A. (1997). *Cig30*, a mouse member of a novel membrane protein gene family, is involved in the recruitment of brown adipose tissue. J. Biol. Chem. **272,** 31738–31746.

Tvrdik, P., Westerberg, R., Silve, S., Asadi, A., Jakobsson, A., Cannon, B., Loison, G., and Jacobsson, A. (2000). Role of new mammalian gene family in the biosynthesis of very long chain fatty acids and sphingolipids. J. Cell Biol. **149,** 707–717.

Ullah, H., Chen, J., Young, J.C., Im, K., Sussman, M.R., and Jones, A.M. (2001). Modulation of cell proliferation by heterotrimeric G protein in *Arabidopsis*. Science. **292,** 2066–2069.

Van Brocklyn, J.R., et al. (1998). Dual actions of sphingosine-1-phosphate: extracellular through G(i)-coupled receptor Edg-1 and intracellular to regulate proliferation and survival. J. Cell. Biol. **142,** 229–240.

Wang, X.-Q., Ullah, H., Jones, A.M., and Assmann, S.M. (2001). G protein regulation of ion channels and abscisic acid signaling in *Arabidopsis* guard cells. Science. **292,** 2070–2072.

Weigel, D., et al. (2000). Activation tagging in *Arabidopsis*. Plant Physiol. **122,** 1003–1013.

Worrall, D., Liang, Y.K., Alvarez, S., Holroyd, G.H., Spiegel, S., Panagopulos, M., Gray, J.E., and Hetherington, A.M. (2008). Involvement of sphingosine kinase in plant cell signalling. Plant J. doi: 10.1111/j.1365–313X.2008.03579.x.

Worrall, D., Ng, C.K.-Y., and Heatherington, A.M. (2003). Sphingolipids, new players in plant signaling. TIPS. **8,** 317–320.

Xiong, L., David, L., Stevenson, B., and Zhu, J.K. (1999). High throughput screening of signal transduction mutants with luciferase imaging. Plant Mol. Biol. Reptr. **17,** 159–170.

Zheng, H., Rowland, O., and Kunst, L. (2005). Disruptions of the *Arabidopsis* Enoyl-CoA reductase gene reveal an essential role for very-long-chain fatty acid synthesis in cell expansion during plant morphogenesis. Plant Cell. **17,** 1467–1481.